JAST, Vol. 7, No. 1, pp 31–40

JAST
Journal of Aerospace Science and Technology

Critical Drag Investigation for an Axisymmetric Projectile with Choked Base Bleed at High-Subsonic and Transonic Regime Using SST K-w Model

M. Saniei Nejad[1], R. Jamshidi[2]

In this following paper, the effects of a choked jet exhausted from the base of a non-lifting body on its total and base drags at sub-sonic and transonic regimes have been numerically investigated. Having surveyed the results of some turbulence models and after comparing with experimental results, an appropriate turbulence model, i.e. SST K-ω, has been chosen and this model has been used in the subsequent analysis. The analysis has been conducted in the free stream Mach number range of 0.4<Ma<0.8, free stream static temperature of 300K, free stream turbulence intensity (Tu) of 2 percent and jet stream turbulence intensity (Tu) of 10 percent. The results showed that, despite of the general supposition among the aerodynamicists, the presence of jet would impose a critical magnitude for the base drag and the total drag as a function of A_j/A_b ratios and free stream Mach numbers; in other words, we have shown that any increase in the jet area or in free stream Mach number, under most conditions decreases the base drag and the total drag of the body and increases them under some conditions.

NOMENCLATURE

A_b	Base Area of the Non-Lifting Body ($=A_{Base}$)
A_j	Jet Area Exhausted from the Base of the Non-Lifting Body ($=A_{Jet}$)
c_p	Thermal capacity at constant pressure
E	Total energy $h-(p/\rho)+(U^2/2)$
F_{Db}	Base Drag Force of the Projectile
F_{Ds}	Surface Drag Force of the Projectile
F_{Dtotal}	Total Drag Force of the Projectile
h	Sensible enthalpy
K	Reynolds average of Turbulent kinetic energy
k	Thermal conductivity
p	Local static pressure
Pr_t	Turbulent prandtl number
R	Gas Constant, R_u/M
r	Radial coordinate in cylindrical system of coordinates
S	Absolute value of strain rate $(2\,S_{ij}\,S_{ij})^{1/2}$
S_{ij}	Strain rate tensor $0.5(\partial u_i/\partial x_j+\partial u_j/\partial x_i)$
T	Local static temperature
Tu	Turbulence intensity, $100(2K/3)^{1/2}/U$
U	Local velocity
u_i	Velocity component in x_i direction
u_i'	Fluctuating velocity component in x_i direction
x_i	Cartesian coordinate component in ith direction
y	Distance to nearest wall
y^+	Distance in wall coordinates, $\rho y\mu\tau/\mu$
μ	Molecular viscosity

1. *M.Sc. Graduate, Dept. of Mech. Eng., Sharif Univ. of Tech., Tehran, Iran.*
2. *B.Sc. Graduate, Dept. of Mech. Eng., Zanjan Univ., Zanjan, Iran.*

μ_t	Eddy viscosity
μ_τ	Friction velocity
ρ	Density
τ	Wall shear stress
τ_{ij}	Deviatoric Tensor
ϵ	Turbulence dissipation rate
ω	Turbulence frequency

INTRODUCTION

One of the important issues in the design of an axisymmetric projectile is to keep its aerodynamic drag as small as possible. The total drag of an axisymmetric projectile consists of three drag components: the pressure drag or the wave drag (excluding the base), the viscous drag, and the base drag. The base drag component is often a large part of the total drag and can be as much as 50% or more than the total drag of a jet-free projectile within a compressible regime. Of all these three components of drag, the most difficult one to predict is the base drag. The base drag depends on the pressure acting on the base. Therefore it is necessary to predict the base pressure as accurately as possible. Figure 1 is a schematic diagram showing the important features of high-subsonic base flow with choked base bleed. The approaching subsonic turbulent boundary layer separates at the base corner, and the free shear layer region is formed in the wake. After separating the flow at the base corner, it is followed by the recirculation zone downstream of the base, which realigns the flow. The flow then redevelops in the trailing wake. In the absence of base bleed, a low-pressure region is formed immediately downstream of the base, which is characterized by a low-speed recirculating flow region. Interaction between this recirculating region and the inviscid external flow occurs through the free shear mixing region. This mixing region is the point where turbulence plays an important role. Injection of choked flow into the base region displaces the entire recirculation region downstream into the wake. The bleed flow results in a change of the base pressure as well as a change in the base drag.

The drag behavior due to base bleed at high-subsonic, transonic and supersonic speeds is of practical importance. The effect of base bleed or mass injection has been studied experimentally and numerically over the past four decades. These studies involved cold and hot gas injection into cylindrical and boat-tailed after-bodies and clearly showed the effectiveness of base bleed on the base pressure. Most of these experimental and numerical investigations were rather limited in nature and lacked measurements of the detailed base pressure distribution and near-wake flow-field such as mean flow and turbulence quantities. Such detailed data have been made available recently for supersonic flow over a cylindrical after-body with base bleed. This set of experimental data not only provides insight into the details of the fluid dynamic interactions in the near wake but also serves as a benchmark for validation of computational results. This paper describes the numerical investigation of the choked bleed jet effects for NASA's experimental model which was conducted in the 1960's without any base bleed. In the following sections, we investigate the critical magnitude of A_j/A_b ratios to have the maximum base and maximum total drag for the mentioned body in different magnitude of free stream Mach number at high-subsonic and transonic free stream regimes.

REVIEW OF PREVIOUS WORKS

Over the past three-decades, the ability to compute the base flow region and it's interaction with other far-field characteristics has advanced. Sahu, Nietubicz and Steger [Ref. 1] examined projectile base flow with and without base flow injection using Navier-Stokes computations. Sahu [Ref. 2,3] performed further calculations of supersonic flow over a missile aft-body containing an exhaust jet and examined the transonic critical aerodynamic behavior. Bartelson and Linde [Ref. 4] proposed a functional relation between the Mach number, the ambient atmospheric pressure and the drag coefficient of a base bleed projectile. Ding, Liu and Chen [Ref. 5] have presented the experimental research results of the drag reduction rate of the base bleed of solid fuel-rich propellent column at subsonic speeds. Fu and Liang [Ref. 6] have numerically investigated a drag reduction method—passive control of shock/boundary layer interaction, which has been applied to the boattail portion of a secant-ogive-cylinder-boattail projectile in turbulent transonic flows. Sahu and Heavey [Ref. 7] compared the results of their computational study to experimental data and found the standard k-ϵ turbulence model performed better in the near wake region than did the algebraic model. Viswanath [Ref. 8] investigated the problem of turbulent base flows and the drag associated with it. He conducted a review of the developments that have taken place on the use of passive techniques or devices for axi-symmetric base and net after-body drag reduction in the absence of jet flow at the base. Kaurinkoski [Ref. 9] has implemented an eddy breakup model for chemical reactions to an existing multi-block Navier-Stokes solver, which has then been used to solve the flow past a supersonic long-range base-bleed projectile. Lee and Kim [Ref. 10] have examined the minimization of base drag using mass bleed control in considering of various base to orifice exit area ratios for a body of revolution in the Mach 2.47 free-stream.

Tanner [Ref. 11] developed a theory to describe the loss of momentum due to the shear stresses in the

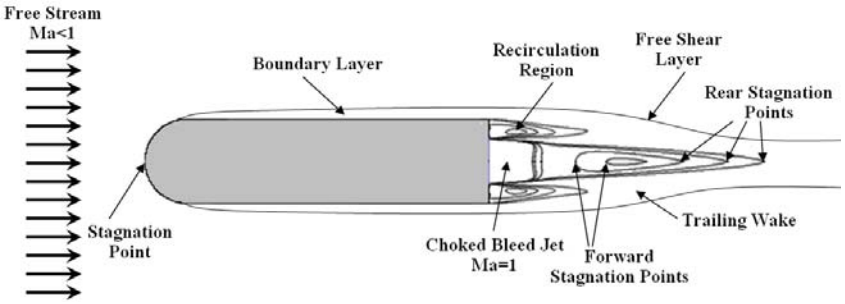

Figure 1. A chematic representation of a high-subsonic base flow with choked mass bleed.

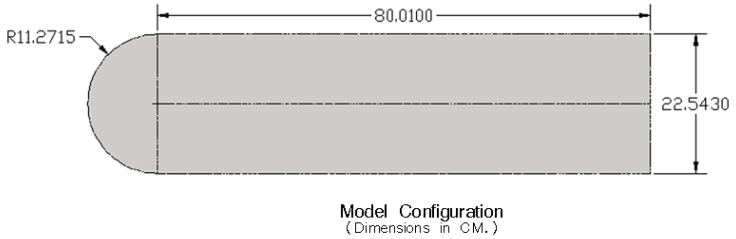

Figure 2. A schematic representation of the non-lifting body and it's dimensions.

near-wake in an incompressible two-dimensional steady base flow.

OBJECTIVE OF THE CURRENT PAPER

The overall objective of the current effort is the numerical investigation of the critical drag of an axisymmetric projectile with choked bleed jet, at which the maximum base drag and the corresponding maximum total drag have been occurred as a function of A_{jet} / A_{base} ratios and also as a function of free stream Mach numbers at high-subsonic and transonic regimes.

PROBLEM DESCRIPTION AND SOLUTION STRATEGY

The dimensions of the investigated model are shown in Figure 2. The standard model is of particular interest in the study of base drag analysis among the aerodynamic research centers and this model has been considered as a benchmark for verifying the results and calibrations of the equipment of any subsonic and transonic wind tunnel and also as a benchmark model for verifying the results and calibrations of the closure-constants of any under-development turbulence model.

In this following paper, a home-made two-dimensional CFD code has been used; of particular interest is the careful characterization of the limited turbulence models employed in this CFD code.

According to Mayle criterion [Ref. 12], for sufficient high speed flows, since natural transition from laminar to turbulent regime would be delayed to downstream of the region of accelerating flow (downstream of nose-body interface), the full turbulent assumption around the nose and initial part of the cylindrical body can be neglected and the flow around this region can be treated as a laminar flow. The flow around the rest of the projectile is considered as a fully turbulent one. To ensure that we have used a reliable CFD method and also a reliable turbulence model, the CFD results of this projectile for jet-free conditions have been compared with NASA's experimental wind tunnel test of the same model at various free stream Mach numbers. These experiments have been conducted in the Langley research center in 1966 [Ref. 13].The inconsiderable errors of the following numerical results in comparison with NASA's available experimental data for the same model and the same flow condition indicate the authenticity of the zonal laminar flow assumption around the nose and also the exactness of the numerical methods which have been used.

After selecting an appropriate and accurate turbulence model for jet-free conditions, the analysis for jet effects has been conducted using the same turbulence model. Since both base-flow and jet-flow can be categorized as shear layer flows, we anticipate similar accuracy in jet-flow condition.

GRID STUDY AND BOUNDARY CONDITIONS

In this present section, we will first verify the code and generated grid by performing grid convergence study

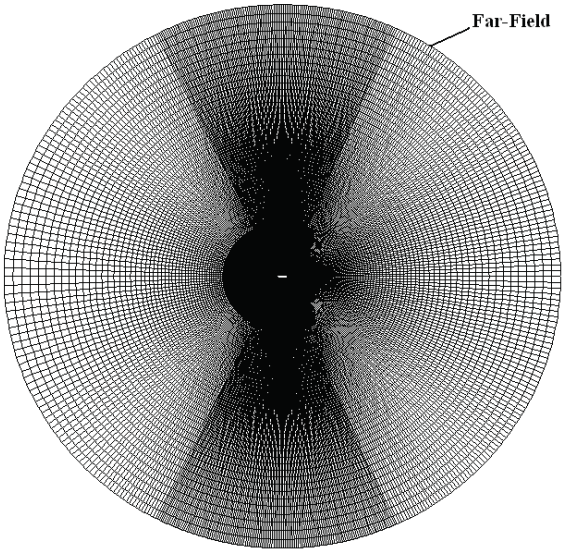

Figure 3. Structured grid generated around the non-lifting body (above) and multi-layer grid refinement used around the model to capture sharp gradients of flow structure into the boundary layer (Bottom).

and comparing it with experimental data for total drag coefficient. Considering the available experimental results of the model [Ref. 13], the numerical analysis of the model had to be done in zero angle-of-attack. Hence, we had to make a two-dimensional axisymmetric computational domain around the model. A schematic representation of the domain and generated structured grid is shown in Figure 3.

At the fluid-solid boundary, non-slip boundary condition has been used. Most computational results of the present study are obtained using grid resolution of about 700,000 grid points to save the computing time and without significant loss of accuracy. It will be shown that the total number of 700,000 elements has required accuracy to have a grid independent solution.

Non-reflection Far-field boundary conditions (B.C.) have been imposed at the inlet and outlet of the computational domain. The boundary condition of the exhausted jet has been chosen as Pressure Inlet. The Mach number and total temperature of the exhausted jet has been set to 1 and 850K respectively. The Mach number of 1 represents the choked condition. It should be noted that the turbulence intensity (Tu) and turbulence length scale for Far-field condition have been set to 2% and 1 mm respectively. Reynolds number for all the following results has been fixed at 6.3 million which is the same magnitude as NASA's flow condition for available data.

Since transition from laminar to turbulent flow can account for significant changes in such important parameters as skin friction, heat transfer, and wake structure, it is important that the transition location (transition from laminar regime to turbulent one) be accurately determined. In this numerical analysis, due to relatively low free stream turbulence level and according to mayle criterion for natural transition inception [Ref. 12], the zone around the nose of the model has been treated as a laminar zone. At relatively high speed accelerating flows, a comprehensive investigation of a large number of transition data [Ref. 14, 15, 16] has shown that the choice of the virtual origin of transition at the point of nose-body interface could give the most consistent results.

GOVERNING EQUATIONS

The continuity equation and Reynolds-averaged Navier-Stokes equations for an axisymmetric domain in a cylindrical system of coordinates are as follows:

$$\frac{\partial \rho}{\partial t} + \frac{\partial}{\partial x}(\rho u_x) + \frac{\partial}{\partial r}(\rho u_r) + \frac{\rho u_r}{r} = 0 \tag{1}$$

$$\begin{aligned}\frac{\partial(\rho u_r)}{\partial t} + \frac{1}{r}\frac{\partial(r\rho u_x u_r)}{\partial x} + \frac{1}{r}\frac{\partial(r\rho u_r u_r)}{\partial r} &= -\frac{\partial p}{\partial r} \\ &+ \frac{1}{r}\frac{\partial}{\partial x}\left[r\mu\left(\frac{\partial u_r}{\partial x} + \frac{\partial u_x}{\partial r}\right)\right] \\ &+ \frac{1}{r}\frac{\partial}{\partial r}\left[r\mu\left(2\frac{\partial u_r}{\partial r} - \frac{2}{3}(\nabla\cdot\vec{u})\right)\right] \\ &- 2\mu\frac{u_r}{r^2} + \frac{2}{3}\frac{\mu}{r}(\nabla\cdot\vec{u}) + \frac{\rho}{r}u_z^2\end{aligned} \tag{2}$$

where

$$\nabla\cdot\vec{u} = \frac{\partial u_x}{\partial x} + \frac{\partial u_r}{\partial r} + \frac{u_r}{r}$$

in which u_z represents the swirl velocity. The energy transport equation (in Cartesian system of coordinates) and state equation which relates the local static pressure to local density and local static temperature are as follows:

$$\begin{aligned}\frac{\partial(\rho E)}{\partial t} + \frac{\partial[u_i(\rho E + p)]}{\partial x_i} \\ = \frac{\partial}{\partial x_j}\left[\left(k + \frac{c_p\mu_t}{\mathrm{Pr}_t}\right)\frac{\partial T}{\partial x_j} + u_i(\tau_{ij})_{eff}\right]\end{aligned} \tag{3}$$

where

$$p = \rho R T \tag{4}$$

In equation (3), k is the thermal conductivity coefficient, E is the total energy and $(\tau_{ij})_{eff}$ is the deviatoric tensor and is defined as follows:

$$(\tau_{ij})_{eff} = \mu_{eff}\left(\frac{\partial u_j}{\partial x_i} + \frac{\partial u_i}{\partial x_j}\right) - \frac{2}{3}\mu_{eff}\frac{\partial u_i}{\partial x_i}\delta_{ij} \tag{5}$$

A complete time-dependent solution of the exact Navier-Stokes equations for high-Reynolds-number turbulent flows in complex geometries is unlikely to be

attainable for some time to come. Hence, Reynolds averaging method can be employed to transform the Navier-Stokes equations in such a way that the small-scale turbulent fluctuations do not have to be directly simulated. This method introduces additional terms in the governing equations that need to be modeled in order to achieve "closure". (Closure implies that there are a sufficient number of equations for all the unknowns.)

The Reynolds-averaged Navier-Stokes (RANS) equations represent transport equations for the mean flow quantities only, with all the scales of the turbulence being modeled. The approach of permitting a solution for the mean flow variables greatly reduces the computational effort. If the mean flow is steady, the governing equations will not contain time derivatives and a steady-state solution can be obtained economically.

REYNOLDS (ENSEMBLE) AVERAGING

In Reynolds averaging, the solution variables in the instantaneous (exact) Navier-Stokes equations are decomposed into the mean (ensemble averaged or time-averaged) and fluctuating components. For velocity components:

$$u_i = \bar{u} + u_i' \tag{6}$$

where $\bar{u}$ and u' are the mean and fluctuating velocity components respectively. Likewise, for pressure and other scalar quantities:

$$\phi = \bar{\phi} + \phi' \tag{7}$$

where ϕ denotes a scalar such as pressure, energy, or species concentration. Substituting expressions of this form for the flow variables into the instantaneous Continuity, momentum (and energy) equations and taking a time (or ensemble) average (and dropping the overbar on the mean velocity, $\bar{u}$) yields the ensemble-averaged momentum (and energy) equations. They can be written (in Cartesian tensor form for instance) as:

$$\frac{\partial \rho}{\partial t} + \frac{\partial}{\partial x_i}\left(\rho u_i\right) = 0 \tag{8}$$

$$\begin{aligned}\frac{\partial \left(\rho u_i\right)}{\partial t} + \frac{\partial \left(\rho u_i u_j\right)}{\partial x_i} &= -\frac{\partial p}{\partial x_i} \\ &+ \frac{\partial}{\partial x_j}\left[\mu\left(\frac{\partial u_i}{\partial x_j} + \frac{\partial u_j}{\partial x_i} - \frac{2}{3}\delta_{ij}\frac{\partial u_\ell}{\partial x_\ell}\right)\right] \\ &+ \frac{\partial}{\partial x_j}\left(-\rho\overline{u_i' u_j'}\right)\end{aligned} \tag{9}$$

As we see, these equations have the same general form as the instantaneous Navier-Stokes equations, with the velocities and other solution variables now representing ensemble-averaged (or time-averaged) values. Additional terms which appeared in the R.H.S. of equation (9) represent the effects of turbulence.

SOLUTION PROCEDURE

The governing equations have been solved using segregated method and the pressure-velocity coupling has been treated as SIMPLEC method. To treat the Reynolds stress terms, $-\rho\overline{u'}_j$, which appeared in the R.H.S. of the equation (9), we have used eddy-viscosity turbulence models, According to authentic references and due to its noticeable capabilities in viscous flows, the SST K-ω turbulence model has been chosen to capture the turbulent quantities with acceptable accuracy particularly in transonic regimes.[Ref. 17, 18, 19].

Boussinesq Approximation

Every turbulence modeling requires that the Reynolds stress terms, $-\rho\overline{u'}_j$, be modeled in an appropriate method. One of the most general methods of modeling this stress term is using Boussinesq approximation in which the magnitude of $-\rho\overline{u'}_j$ is related to velocity gradients within the computational domain. In Cartesian system of coordinates, we have the following relation between Reynolds stress and available gradients of velocities:

$$-\rho\overline{u_i' u_j'} = \mu_t\left(\frac{\partial u_i}{\partial x_j} + \frac{\partial u_j}{\partial x_i}\right) - \frac{2}{3}\left(\rho K + \mu_t\frac{\partial u_i}{\partial x_i}\right)\delta_{ij} \tag{10}$$

in which K represents the turbulent kinetic energy, $K = \overline{u_i' u_i'}$. To compute the turbulent viscosity, μ_t, or equivalently $\nu_t \equiv \mu_t/\rho$, we need to use appropriate turbulence models.

SST K-ω model Formulation

In the following paragraphs, we consider the details of SST K-ω model which is a powerful one to capture the flow physics in both high Reynolds number region away from the wall and low Reynolds number close to the wall. This model also has some vantages over other classic turbulence models, such as standard K-ϵ and standard K-ω.

The SST turbulence model (Menter, Ref. 18) has been used to compute the turbulent viscosity (μ_t) that is present in the momentum and energy equations in order to model the effects of turbulence on the flow correctly. The SST model combines the advantages of the K-ω in high Reynolds number flow (away from solid surfaces) and the K-ω model (close to solid surfaces) to achieve an optimal model formulation for a wide range of applications (Menter, 1994). For this reason, a blending function F1 is introduced which is equal to one near the solid surface and equal to zero for the flow domain away from the wall. It activates the $K-\omega$ model in the near wall region and the $K-\epsilon$ model for the rest of the flow. By this approach the attractive near-wall performance of the $K-\omega$ model can be used without the potential errors resulting from the free stream sensitivity of that model. In addition, the

SST model also features a modification of the definition of the eddy viscosity, which can be interpreted as a variable c_μ, where c_μ in the $K-\epsilon$ model is constant. This modification is required to accurately capture the onset of separation under pressure gradients. The modeled equations for the turbulent kinetic energy, K, and the turbulence frequency ω in Cartesian system of coordinate are as follows:

$$\frac{\partial \rho K}{\partial t} + \frac{\partial}{\partial x_j}\left(\rho\, \bar{u}_j K\right) = P_K - D_K + \frac{\partial}{\partial x_j}\left(\Gamma_K \frac{\partial K}{\partial x_j}\right) \tag{11}$$

$$\frac{\partial \rho \omega}{\partial t} + \frac{\partial}{\partial x_j}\left(\rho\, \bar{u}_j \omega\right) = \frac{\gamma}{\nu_t} P_K - \beta \rho \omega^2 + \frac{\partial}{\partial x_j}\left(\Gamma_\omega \frac{\partial \omega}{\partial x_j}\right) + \left(1 - F_1\right) 2\rho\sigma_{\omega 2} \frac{1}{\omega} \frac{\partial K}{\partial x_j} \frac{\partial \omega}{\partial x_j} \tag{12}$$

in which, Γ_K and Γ_ω represent effective diffusivity of K and ω respectively. The production and destruction terms for the turbulence kinetic energy equation are defined as:

$$P_K = \min\left(\mu_t S^2, 10 D_K\right) \tag{13}$$

$$D_K = \beta^* \rho \omega K \tag{14}$$

and the blending function F_1 is calculated from:

$$F_1 = \tanh\left(\arg_1^4\right) \tag{15}$$

$$arg_1 = \min\left(\max\left(\frac{\sqrt{K}}{\beta^* \omega y}, \frac{500\nu}{\omega y^2}\right), \frac{4\rho\sigma_{\omega 2} K}{CD_{K\omega} y^2}\right) \tag{16}$$

$$CD_{K\omega} = \max\left(2\rho\sigma_{\omega 2} \frac{1}{\omega} \frac{\partial K}{\partial x_j} \frac{\partial \omega}{\partial x_j}, 1.e^{-10}\right) \tag{17}$$

The turbulent viscosity is then calculated by:

$$\mu_t = \min\left(\frac{\rho K}{\omega}, \frac{a_1 \rho K}{S F_2}\right) \tag{18}$$

with the constant $a_1 = 0.31$ and the blending function F_2 obtained from:

$$F_2 = \tanh\left(\arg_2^2\right) \tag{19}$$

$$\arg_2 = \max\left(\frac{2\sqrt{K}}{\beta^* \omega y}, \frac{500\nu}{\omega y^2}\right) \tag{20}$$

It should be noted that, for laminar zone around the nose, we have set $\mu_t = \mu$. The coefficients, φ of the model, are functions of F_1: $\varphi = F_1\varphi_1 + (1\text{-}F_1)\varphi_2$ where φ_1, φ_2 stand for the coefficients of the $K-\omega$ and the $K-\epsilon$ model respectively:

$\sigma_{K1} = 1.176$, $\sigma_{\omega 1} = 2.0$, $\kappa = 0.41$,

$\gamma_1 = 0.5532$, $\beta_1 = 0.075$, $\beta^* = 0.09$, $c_1 = 10$

$\sigma_{K2} = 1.0$, $\sigma_{\omega 2} = 1.168$, $\kappa = 0.41$,

$\gamma_2 = 0.4403$, $\beta_2 = 0.0828$, $\beta^* = 0.09$

Now, we have to investigate the authenticity of the used numerical methods and turbulence models and multi-zone domain decomposition technique, i.e. implementing laminar zone around the nose and full turbulent zones for the rest of the domain on the accuracy of the results in a jet-free condition (100 percent base drag). To this end, the results have been compared with NASA's experimental study which was conducted at Mach number ranges from 0.2 to 0.8 and Reynolds number of 6.3 million [Ref. 13].

Check for convergence

There are no universal metrics for judging convergence. Residual definitions useful for one class of problems are sometimes misleading for other classes of problems. Therefore, it is a good idea to judge convergence not only by examining residual levels, but also by monitoring relevant integrated quantities (such as drag forces

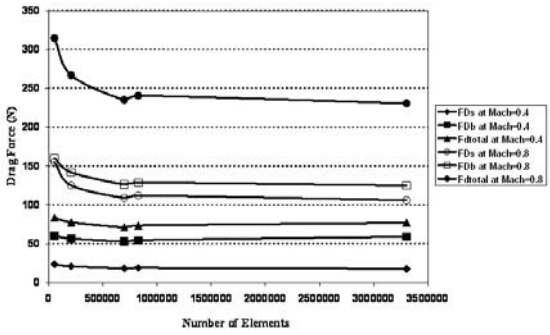

Figure 4. Grid independency check for different element numbers at different free stream Mach numbers.

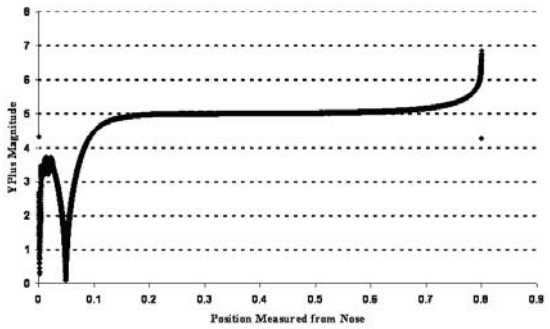

Figure 5. y^+ distribution over the nose and cylindrical part of the non-lifting body.

exerted over some parts of the body) and checking for mass and energy balances.

The three methods to check for convergence are:

- Monitoring the residuals.
  Convergence will occur when the convergence criterion for each variable has been reached. The default criterion is that each residual will be reduced to a value of less than 10^{-5}, except the energy residual, for which the default criterion is 10^{-9}.
- Solution no longer changes with further iterations.
  Sometimes the residuals may not fall below the convergence criterion. However, monitoring the representative flow variables through iterations may show that the residuals have stagnated and do not change with further iterations. This could also be considered as convergence.
- Overall mass, momentum, energy and scalar balances are obtained.
  One of the criteria of convergence is that the net imbalance should be less than 0.1% of the net flux through the domain.

We have used all of the above methods of convergence check beside appropriate grid adaptation techniques (based on the converged results of previous coarse grid level) to achieve the best and the most accurate numerical solutions.

Grid convergence study and comparison between experimental and numerical results

At the first step, we had to prove the grid independency of the solutions acquired using grid generated with 700,000 elements. It's shown in Figure 4 that the grid independency check of the solutions for different element numbers which was converged at different free stream Mach numbers. Also Figure 5 shows the density and distribution of the cells which are enough to have maximum wall y^+ of 6 for all the free stream Mach number ranges. They are also in an acceptable range for every turbulence model such as K-ω SST which doesn't use wall functions. The comparison between total drag from both wind tunnel and converged CFD results is plotted in Figure 6; it should be mentioned that the experimental results had an error of$\pm$ 0.043 in Mach number of 0.2 and $\pm$0.003 in Mach number of 0.8.

Having considered a linear variation of errors for other Mach numbers, the hatched zone in Figure 6 is a valid zone for total drag for every other Mach numbers in subsonic and transonic regimes. As illustrated in Figure 6, the numerical results have reasonable accuracy in capturing and computing the overall drag of the body in all of the Mach numbers.

To evaluate the accuracy of the numerical results of the base drag and surface drag, where the latter

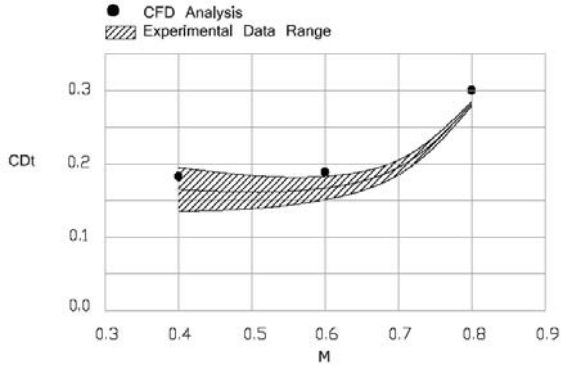

Figure 6. Comparison between numerical and experimental values of total drag coefficient at various Mach numbers.

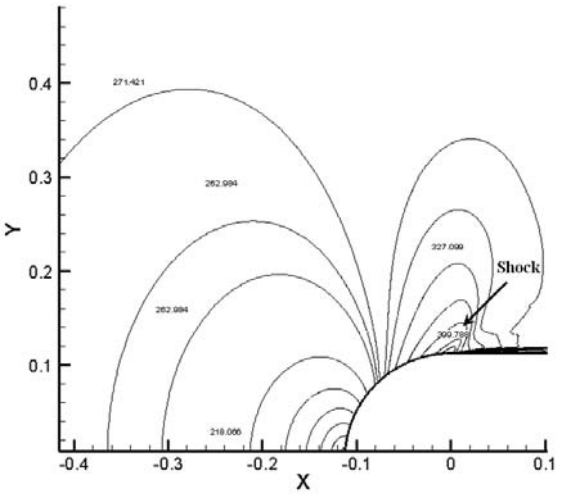

Figure 7. Shock generated at the position of nose-cylindrical body interface at Mach=0.8.

includes nose and cylindrical body drag, the related coefficients have been compared with experimental results in tables [1] and [2]:

It should be noted that the relative errors in tables [1] and [2] have been computed without considering the errors of measurements and calibrations. It's obvious

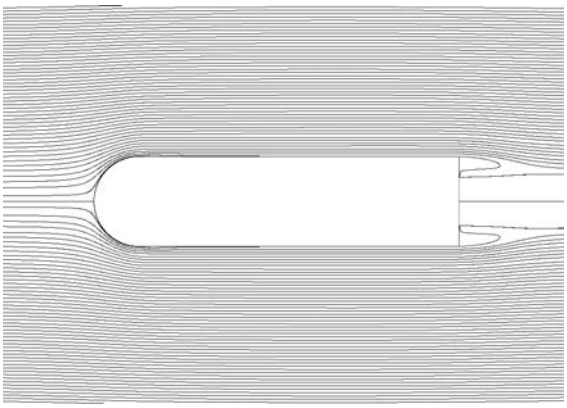

Figure 8. Contours of Pathlines for A_{Jet}/A_{Base} =0.283 at Mach=0.8.

Table 1. Comparison between numerical and experimental results of the base drag Coef., CD_b.

Relative Erorr (%)	CD_b (CFD)	CD_b (Experiment)	Mach Number
17.4	0.135	0.115	0.4
20.5	0.141	0.117	0.6
22.7	0.162	0.132	0.8

Table 2. Comparison between numerical and experimental results of the surface drag Coef., CD_s.

Relative Erorr (%)	CD_s(CFD)	CD_s(Experiment)	Mach Number
6	0.047	0.05	0.4
4	0.048	0.05	0.6
7.3	0.139	0.15	0.8

that after considering the errors of measurements and calibrations, the values of errors in above tables would be decreased substantially.

After these comparisons, we can use SST K-ω model as a verified turbulence model with acceptable accuracy in capturing the shear layer flows around the projectile in both high-subsonic and transonic regimes.

According to the acquired results with acceptable accuracy, we can now activate the jet exhausted from the base of the body, and investigate the effect of jet area over the base drag and total drag of the mentioned body. Since both base-flow and jet-flow can be categorized as shear layer flows, we expect to have similar accuracy in jet-flow CFD analysis.

The jet has a Mach number of 1, which is an appropriate condition for choked flow, and has a total temperature of 850K. The free stream turbulence and the turbulence length scale have been set to 2 percent and 1mm respectively.

Some contours of the converged results are shown in Figures 7,8. As can be seen in Figure 7, due to flow acceleration, shock has been generated at the position of nose-cylindrical body interface at free stream Mach number of 0.8, which is an indication of transonic regime. Downstream of the shock, because of the interaction between shock and boundary layer, a local boundary layer separation had occurred which disappeared at a short distance due to turbulent flow reattachment effect.

The results of the base drag and surface drag for different free stream Mach numbers and different values of A_{Jet}/A_{Base} are plotted in Figures 9,10 and 11. It can be seen that any increase in the jet area not only necessarily decreases the base drag, but also increases the base drag under some conditions. Also what can be seen in Figure 12 is that the peak value of the drag shifts toward lower values of A_{Jet}/A_{Base} with increasing free stream Mach number. Considering the

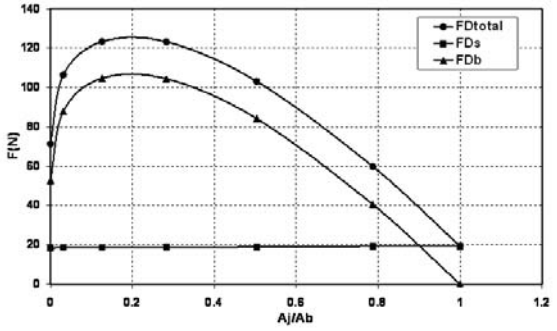

Figure 9. Drag force variation at different ratios of A_{Jet}/A_{Base} , free stream Mach number=0.4.

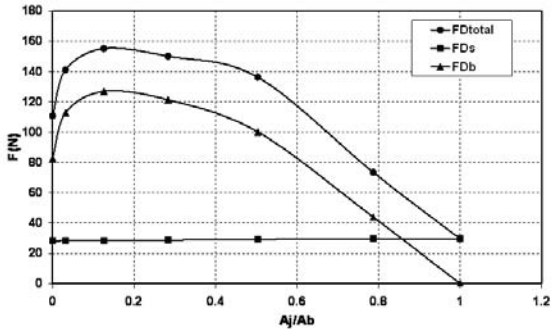

Figure 10. Drag force variation at different ratios of A_{Jet}/A_{Base} , free stream Mach number=0.6.

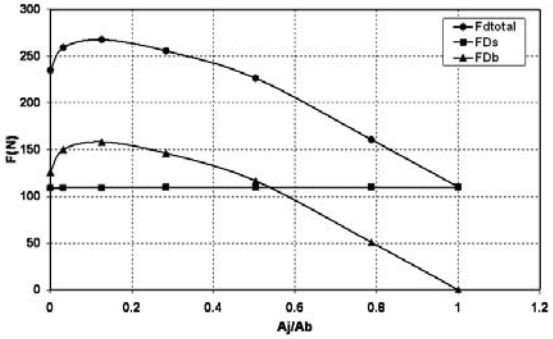

Figure 11. Drag force variation at different ratios of A_{Jet}/A_{Base} , free stream Mach number=0.8.

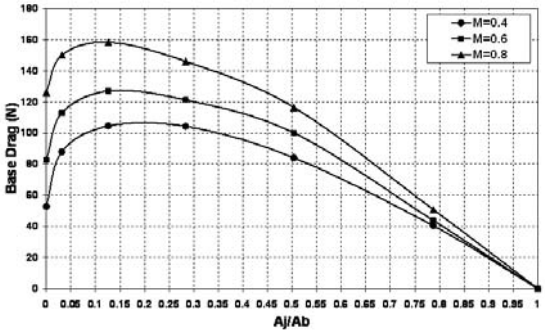

Figure 12. Base drag force variation with A_{Jet}/A_{Base} at various free stream Mach numbers.

peak values of drag and related values of A_{Jet}/A_{Base} is essential in aerodynamic design and optimization of missiles, rockets and also in power-on projectiles. By avoiding these peak values, one can increase the total range of a missile, a rocket or a power-on projectile. In other words, if anyone wants to increase the total range of a power-on missile or rocket in the high-subsonic and transonic regimes, the magnitude of the jet area should be larger or smaller than these critical values of A_{Jet}/A_{Base}. These critical values are also a function of Mach number. Considering these critical values is vital in aerodynamical designs or and particularly in optimum drag reduction of missiles, rockets and power-on projectiles to avoid any increase in total mass and also to avoid any increase in fuel (solid or liquid) consumption.

CONCLUSION

Normally, we expect that after any increase in the jet area exhausted from the base region of a high-speed projectile, the base drag should be decreased. But we always have to consider the shear effects of the exhausted jet on a large portion of flow pattern around the body. This jet would impose a shear velocity profile on the flow layers around the base region and this leads to formation of a local suction (reduction in local static pressure) around the base region. The magnitude of this suction is completely a function of the free stream Mach number and mass flow rate of the exhausted jet. This suction could be so powerful that the base drag of the body, instead of decreasing, would increase.

It's shown in this paper that any increase in the jet area, not only necessarily decreases the base drag, but also increases it in some fluid flow and geometrical conditions. In this regard, we have shown that for every free stream Mach number, we have a critical magnitude for A_{Jet}/A_{Base} in which the surface drag and corresponding total drag are at maximum levels. Also, it is shown that for high-subsonic and transonic regimes, the peak value of the drag shifts toward lower values of A_{Jet}/A_{Base} with increasing free stream Mach numbers.

REFERENCES

1. Sahu J., Nietubicz C., and Steger J., "Navier-Stokes Computations of Projectile Base Flow With and Without Base Injection", *AIAA Journal*, **23**(9), PP 1348-1355(1985).
2. Sahu J., "Supersonic Flow Over Cylindrical After-Bodies with Base Bleed", *AIAA Paper No. 86-0487, Proceedings of the 34th Annual Aerospace Sciences Meeting*, (9861).
3. Sahu J., "Numerical Computations of Transonic Critical Aerodynamic Behavior", *AIM Journal*, **28**(5), PP 807-816(990).
4. Bartelson N., Linde S., "A Model of the Axial Drag Coefficient for Base Bleed Projectiles ", *International Journal of Energetic Materials and Chemical Propulsion*, **1**(1-6), (1991).
5. Ding Z., Liu Y., Chen S., "A Study of Drag Reduction by Base Bleed at Subsonic Speeds ", *International Journal of Energetic Materials and Chemical Propulsion*, **1**(1-6), (1991).
6. Fu J.K., "Numerical Study Of Optimal Drag Reduction For Turbulent Transonic Projectiles Using A Passive Control ", *International Journal of Computational Fluid Dynamics*, **3**(3), PP 251- 264(1994).
7. Sahu J., and Heavey K., "Computational Study of Base Bleed Flow with Experimental Data", *16th Int. Symposium on Ballistics*, (1996).
8. Viswanath P.R., "Flow Management Techniques for Base and After-Body Drag Reduction", *Progress in Aerospace Sciences*, **32**(2-3), PP 79-129(1996).
9. Kaurinkoski P., "Simulation of the Flow Past a Long-Range Artillery Projectile ", *Dissertation for the degree of Doctor of Science in Technology*, (2000).
10. Lee Y.K., Kim H.D., "Optimization of Mass Bleed Control for Base Drag Reduction of Supersonic Flight Bodies", *Journal of Thermal Science*, **15**(3), PP 206-212(2000).
11. Tanner M., "A Theory for Incompressible Two-Dimensional Steady Base Flow with Application to Two Different Problems ", *Aerospace Science and Technology*, **7**(5), PP 340-351(2003).
12. Mayle R.E., "A Theory for Predicting the Turbulent-Spot Production Rate", *Journal of TurboMachinery*, **121**, PP 588-593(1999).
13. Norris J.D. and McGhee R.J., "Effects of Bluntness on the Subsonic Drag of an Elliptical Forebody", *Langley Research Center, NASA*, (1966).
14. Abu-Ghannam B.J. and Shaw R., "Natural Transition of Boundary Layers -The Effects of Turbulence, Pressure Gradient, and Flow History", *Journal of Mechanical Engineering Science*, **22**(5), PP 213 - 228(1980).
15. Dhawan D. and Narasimha R., "Some Properties of Boundary Layer Flow During Transition from Laminar to Turbulent Motion", *Journal of Fluid Mechanics*, **3**, PP 418-436(1958).
16. Durbin P.A., Jacobs R.G. and Wu X., *DNS of Bypass Transition*, Closure Strategies for Turbulent and Transitional Flows, edited by B.E. Launder and N.D. Sandham, Cambridge University Press, (2002).
17. Kim S.E., Choudhury D. and Patel B., "Computations of Complex Turbulent Flows Using the Commercial Code FLUENT", *In Proceedings of the ICASE/LaRC/AFOSR Symposium on Modeling Complex Turbulent Flows* , (1997).
18. Menter F.R., "Two-Equation Eddy-Viscosity Turbulence Models for Engineering Applications", *AIAA Journal*, **32**(8), PP 1598-1605(1994).

19. Reynolds W.C., "Fundamentals of Turbulence for Turbulence Modeling and Simulation", *Lecture Notes for Von Karman Institute Agard Report No. 755*, (1987).